ELSEVIER

Intermetallics 7 (1999) 153–162

Intermetallics

Oxide scale formation and isothermal oxidation behavior of Mo–Si–B intermetallics at 600–1000°C

M.K. Meyer *, A.J. Thom, M. Akinc

Ames Laboratory and Department of Materials Science and Engineering, Iowa State University, Ames, IA 50011, USA

Received 19 May 1997; accepted 10 March 1998

Abstract

Initial scale formation in the range 600–1000°C and isothermal oxidation behavior at 1000°C was investigated for Mo–Si–B intermetallics containing 81–88 wt% molybdenum. All compositions exhibited an initial transient oxidation period consisting of a mass gain due to MoO_3 and SiO_2 formation, followed by a rapid mass loss starting at 750°C due to MoO_3 volatilization. After the initial transient oxidation period, oxidation proceeded at a much slower rate. During isothermal oxidation at 1000°C the oxidation rate was found to vary inversely with the ratio of B/Si in the intermetallic, indicating that viscous flow of the scale was an important factor in determining the isothermal oxidation rate at 1000°C. © 1999 Elsevier Science Ltd. All rights reserved.

1. Introduction

Mo_5Si_3 based materials are candidates for high temperature applications where good creep resistance is required. The creep resistance of Mo_5Si_3 has been shown to be better than that of $MoSi_2$ at 1200°C. [1] However, Mo_5Si_3 has poor high temperature oxidation resistance, with a mass loss rate on the order of 100 $mg\,cm^{-2}\,h^{-1}$ at 1200°C. [2]

The conditions necessary for oxidation of the metal in a metal silicide that forms a coherent scale have been discussed by several authors in relation to silicide coatings on silicon substrates. [3,4] Bartlett et al. [5] used this approach to explain the poor oxidation resistance in Mo_5Si_3, in contrast to the excellent oxidation resistance of $MoSi_2$. Mo_5Si_3 was oxidized between 450 and 1500°C in the oxygen partial pressure range of 10^1–10^5 Pa. Protective scale formation did not occur at atmospheric oxygen pressure (P_{O_2}), but did occur at lower P_{O_2}. Silicon depletion at the oxidation interface due to slow silicon diffusion (D_{Si}) from the matrix was modeled as the cause of oxidative instability. Increasing temperature was correlated with an increase in D_{Si}, thereby combining to increase silicon activity at the interface and decrease P_{O_2} to prevent oxidation of molybdenum.

Berkowitz-Mattuck and Dils [6] studied the oxidation of Mo_5Si_3 by monitoring oxygen consumption during oxidation at temperatures of 1107–1737°C and oxygen pressures of 1082–1750 Pa (8.5–13.1 Torr). Oxidation times were 80–110 min. At 1107 and 1137°C, oxygen consumption was rapid over the duration of the oxidation test, indicating active oxidation and non-protective scale formation. Above 1377°C, specimens exhibited a plateau region of slow oxygen uptake after an initial transient period of rapid oxidation. Total oxygen consumption decreased as oxidation temperature increased. High temperature passivation was proposed to be due to the temperature dependent lateral flow of SiO_2 to form a continuous passivating layer.

Previous work in our laboratory [2] has shown that boron additions in the range 1–2 wt% improve the oxidation resistance of Mo_5Si_3 by about five orders of magnitude at 1200°C. The present work elaborates on the mechanism of oxidation protection afforded by boron additions to the Mo–Si system in the vicinity of the Mo_5Si_3 phase field. Scale formation behavior and oxidation kinetics are examined as a function of composition for materials with 81–88 wt% molybdenum content.

2. Experimental procedure

2.1. Preparation of oxidation coupons

Mo–Si–B intermetallics were synthesized by arc melting of the elements in a non-consumable tungsten arc

* Corresponding author at: Argonne National Laboratory-West, Idaho Falls, ID 83403, USA.

0966-9795/99/$—see front matter © 1999 Elsevier Science Ltd. All rights reserved
PII: S0966-9795(98)00058-2

melt furnace under argon atmosphere. Arc melt buttons were ground in air to submicron size powders in a tungsten carbide lined impact mill (Model 2000 Mixer/Mill, SPEX Industries, Edison, NJ). Powders were sieved through a 635 mesh screen (< 20 μm) after milling and pressed into 0.95 cm diameter pellets at 50 MPa. Pellets were then sintered under high purity argon at 1800°C for 2 h to a density greater than 90% of theoretical. To further increase density, samples were hot isostatically pressed (HIP) at 1750°C and 280 MPa without encapsulation. After HIP, samples were annealed at 1600°C for 24 h under high purity argon to promote chemical and microstructural homogeneity. Phase arrays were determined by using X-ray diffraction (XRD, XDS 2000, Scintag USA, Sunnyvale, CA), scanning electron microscopy (SEM, JSM 6100, JEOL USA, Peabody, MA), and energy dispersive spectroscopy (EDS, Oxford Instruments, Oak Ridge, TN). Specimens used for SEM/EDS examination were etched with Murakami's etch to better differentiate between T2 ($Mo_5(Si,B)_3$) and Mo_3Si phases, which have nearly the same BSE contrast. The etch selectively attacks the T2 and MoB phases. Chemical analysis was determined by ICP–AES (Inductively Coupled Plasma–Atomic Emission Spectroscopy).

Oxidation coupons 1 mm thick were cut from pellets using a diamond saw. Coupons were polished in successive steps to 0.3 μm alumina and ultrasonically cleaned in deionized water. Specimens were then rinsed successively in ethanol, acetone, and hexane and dried at 105°C in air before high temperature oxidation.

2.2. High temperature oxidation

Two types of oxidation experiments were conducted. The first experimental set was designed to allow the observation of scale formation as a function of temperature from 600 to 1000°C. Oxidation coupons were placed on edge in alumina boats inside a quartz tube. The tube and contents were purged with high purity synthetic air (HP air) for 2 h prior to oxidation. Gas flow rate and tube diameter were constant for all experiments. Coupons were heated at a rate of $10°C\,min^{-1}$ until the desired oxidation temperature was reached. At this temperature the quartz tube was immediately slid through the tube furnace to remove the designated coupon from the hot zone. In this way, samples were rapidly quenched from the oxidation temperature. Some specimens were oxidized isothermally at 1000°C for 20 and 40 min before quenching. Gas flow was counter current to tube movement so that volatile oxidation products did not condense on the samples after removal from the hot zone.

The second experimental set involved thermo-gravimetric oxidation experiments to observe transient mass change behavior and to determine isothermal oxidation rates. Coupons were suspended from a sapphire wire in a vertical tube thermo-gravimetric analyzer (System 3, Cahn Instruments, Cerritos, CA). A small hole was spark machined through coupons prior to polishing from which the coupons were suspended. The specimen chamber was purged for 2 h with HP air before each run. Specimen temperature was then increased at a rate of $20°C\,min^{-1}$ to the oxidation temperature and held for 100 h. Specimen mass change and temperature were continuously recorded.

Following oxidation, samples were characterized for scale composition and microstructure using SEM/EDS and XRD.

3. Results

3.1. Microstructures of oxidation coupons

Results of chemical and qualitative microstructural analysis for the five compositions examined in this work are given in Table 1. (Typical impurity analysis is given elsewhere. [2]) The uncertainty in the chemical analysis is a maximum of ±3% by weight of the stated values in Table 1. For example, composition V has the following chemistry and associated uncertainties: Mo = 88.2 ± 2.6 (0.03×88.2), Si = 10.8 ± 0.32, B = 1.0 ± 0.030. The actual molybdenum content variation is much smaller than that suggested by chemical analysis. Evidence for lower uncertainty values in molybdenum analysis is provided by the phase analysis. A variation of 3 wt% in molybdenum content could potentially shift each composition in Table 1 outside the phase triangle in which each composition is known to exist. The maximum uncertainty in molybdenum content is probably closer to ±0.5 wt%. Uncertainties given for silicon and boron content are more reasonable.

Compositions given in Table 1 were chosen in order to vary the phase assemblage of the microstructure, total atomic fraction of boron and silicon relative to molybdenum, and the ratio of boron to silicon. Compositions I and II have the lowest molybdenum and highest silicon levels but differ substantially in boron content (see Table 1). Both compositions I and II (Fig. 1) are three phase mixtures with a Mo_5Si_3 (M) matrix and MoB (A) and $MoSi_2$ (B) as intermetallic second phases. Composition II has $MoSi_2$ as the primary second phase, although a few MoB grains (not shown) were identified using EDS. Composition III contains a Mo_5Si_3 matrix with MoB as the primary second phase, with little $MoSi_2$ present. Composition IV is a Mo_5Si_3 matrix material with Mo_3Si (C) and a ternary $Mo_5(Si,B)_3$ (T2 phase, D) as dispersed phases. Composition V is a Mo_3Si matrix material with T2 and Mo_5Si_3 as major second phases. XRD also indicated that a small amount of metallic molybdenum is present in the

microstructure as a non-equilibrium phase. All compositions contained a silicate glass phase (G), that formed in spherical particles.

3.2. Formation of oxide scale

The development of the oxide scale morphology showed significant differences with changes in specimen composition. Only the analysis of scale evolution for two compositions are presented here for the sake of brevity. Fig. 2 shows SEM surface micrographs of the evolution of the oxide scale on Composition V. At 600°C (Fig. 2(a)), the scale is composed of three distinct areas, mirroring the makeup of the substrate. Small pockets of borosilicate glass appear as the dark phase (c) in the micrograph. Regions of almost pure molybdenum oxide (a) are found both adjacent to the glassy phase and as isolated regions surrounded by a matrix

Table 1
Composition and phase array of Mo–Si–B intermetallics

Specimen	Chemical analysis[a] (wt%)			Phase array[b]				
	Mo	Si	B	Mo_5Si_3	T2	Mo_3Si	$MoSi_2$	MoB
I	81.2	18.2	0.61	+ + +			+	+
II	81.5	18.3	0.14	+ + +			+	+
III	82.2	16.9	0.91	+ + +			+	+ +
IV	86.3	12.6	1.1	+ + +	+ +	+ +		
V	88.2	10.8	1.0	+ +	+ +	+ + +		

[a] All compositions ±3 wt% relative to element being measured.
[b] + + + = matrix phase, + + = major phase, + = minor phase.

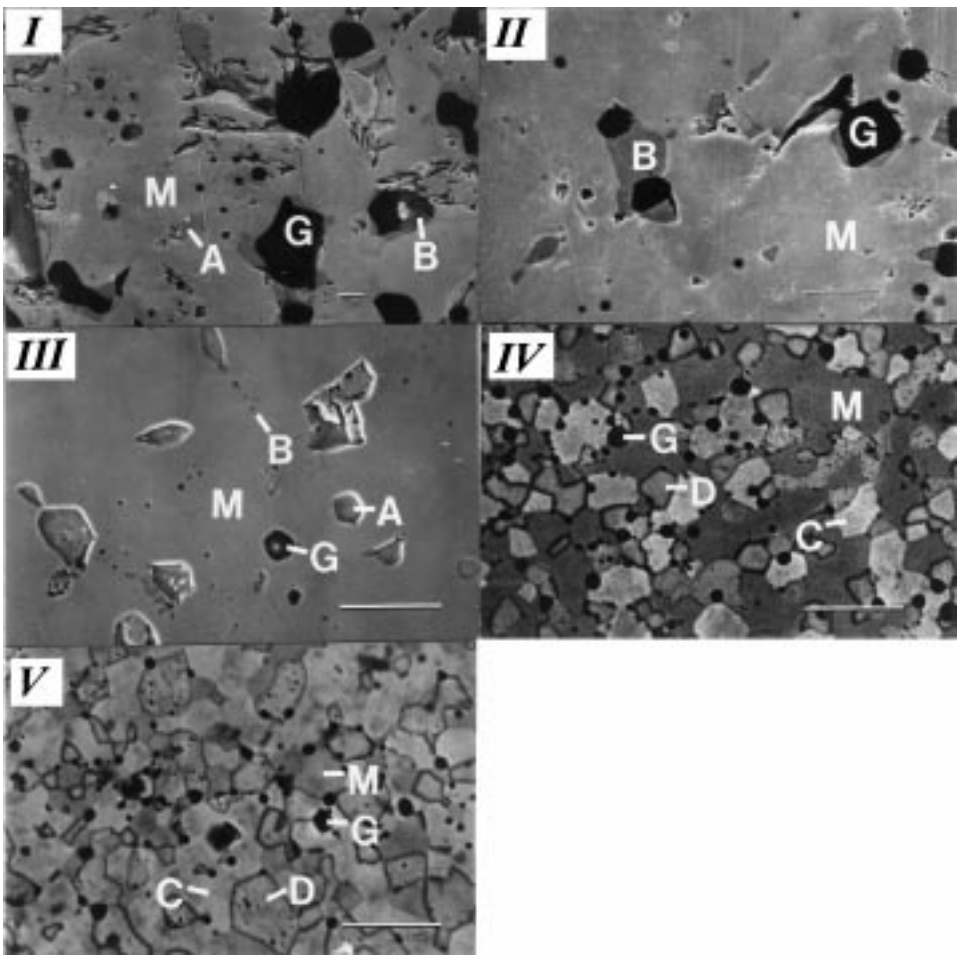

Fig. 1. SEM microstructures of compositions I–V prior to oxidation. See Table 1 for chemical analysis and phase array for compositions I–V. Micrograph labeling key: A = MoB, B = $MoSi_2$, C = Mo_3Si, D = T2 [$Mo_5(Si,B)_3$], G = silica glass, M = Mo_5Si_3. Scale bar = 10 μm.

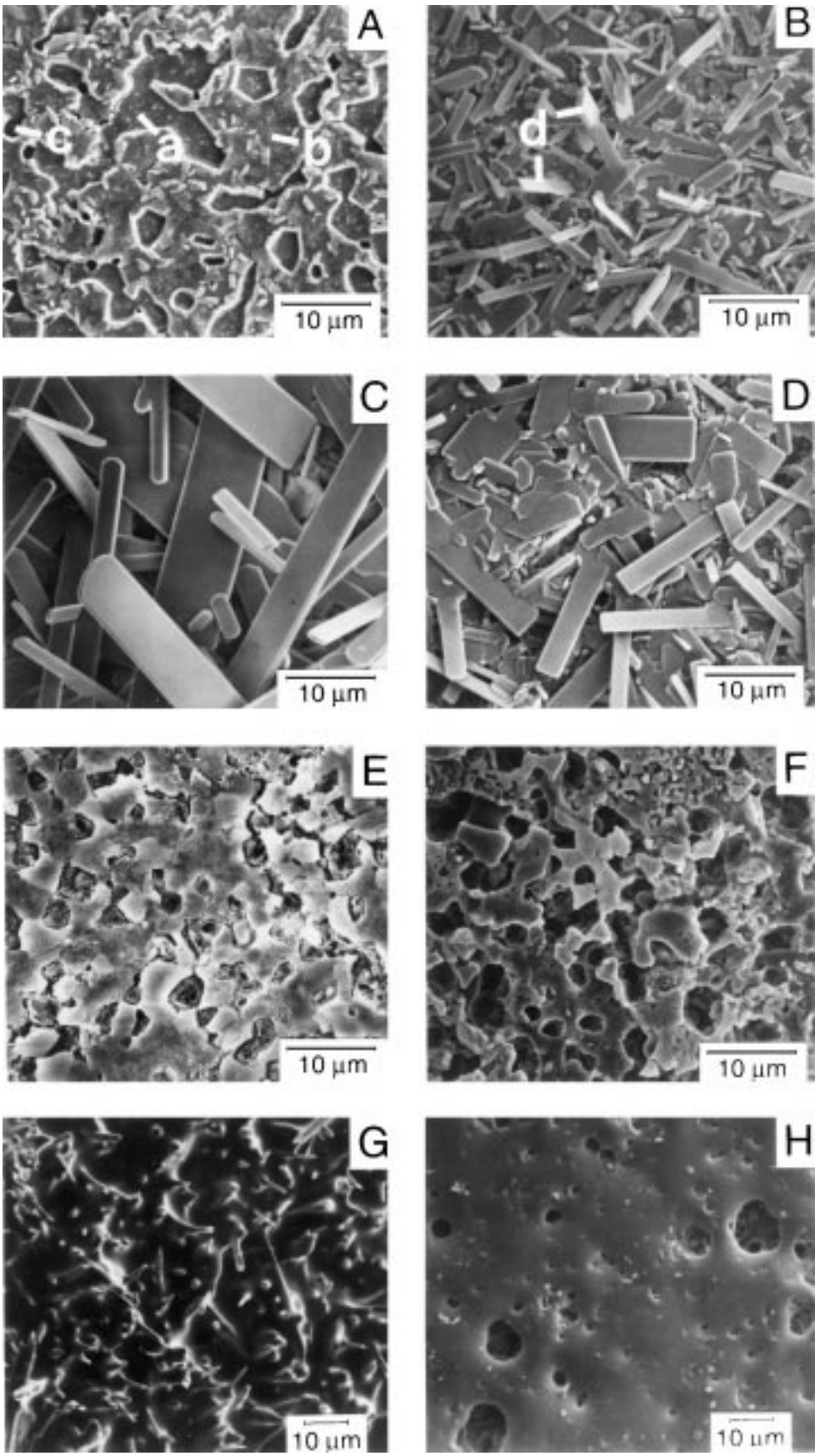

Fig. 2. Formation of the oxide scale on composition V at 600–1000°C. (A) 600°C, (B) 667°C, (C) 725°C, (D) 750°C, (E) 775°C, (F) 1000°C, (G) 1000°C for 20 min, (H) 1000°C for 40 minutes. Labeling key: a = MoO_3, b = $MoO_3 + SiO_2$, c = borosilicate glass, d = MoO_3 crystals.

(b) of mixed molybdenum and silicon oxides. XRD (Fig. 3) does not show any well crystallized molybdenum or silicon oxide at 600°C. The (100) diffraction maxima at 40.5° 2Θ due to metallic molybdenum disappears after oxidation at 600°C indicating that the small amount of metallic molybdenum originally present has been depleted by oxidation in the near surface regions. At 633°C (micrograph not shown), larger MoO_3 crystals begin to form in the scale around the pockets of 'pure' molybdenum oxide. The XRD pattern at 633°C shows peaks due to MoO_3 (Fig. 3). The growth of MoO_3 crystals over the scale surface continues at 667–725°C, as shown in Fig. 2(b) and (c) and Fig. 3. At 750°C, MoO_3 begins to sublime, and the number and size of MoO_3 crystals decreases (Fig. 2(d)). As temperature is increased to 775°C, MoO_3 crystals cover only about one-half of the surface, with the remainder of the surface being composed of porous borosilicate glass with a lacy network structure, as seen in Fig. 2(e). At 1000°C the diffraction maxima for Mo (100) reappears in the spectrum. A sample cooled immediately after heating to 1000°C (Fig. 2(f)) shows signs of viscous flow, as evidenced by the dulling of edges and closure of submicron scale porosity. On holding isothermally for 20 min at 1000°C, (Fig. 2(g)) it can be seen that significant viscous flow has occurred. Molybdenum oxide crystals can be seen growing out of the scale over much of the surface, in accord with observations of mass loss during the initial minutes of isothermal oxidation at 1000°C (see below). The coexistence of MoO_3 and metallic molybdenum indicates that molybdenum is being actively oxidized over part of the coupon, while being protected from oxidation in other areas. After 40 min at 1000°C, the scale appears as shown in Fig. 2(h). There are no longer any signs of MoO_3 formation. The Mo (100) peak grows in intensity with time at 1000°C relative to neighboring Mo_5Si_3, T2, and Mo_3Si intermetallic peaks near 41° 2Θ. These observations provide evidence that the oxidation interface is enriched in molybdenum due to selective oxidation of silicon over molybdenum during passivating scale growth.

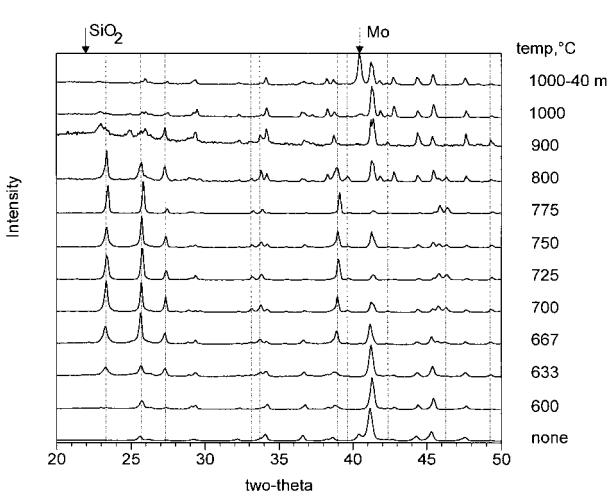

Fig. 3. X-ray diffraction patterns of scale on composition V after oxidation at 600–1000°C. Dashed lines indicate MoO_3. Also indicated are positions of 100% intensity peaks for molybdenum and cristobalite.

Fig. 4 shows the series of micrographs for the oxidation of composition III as a function of temperature. After heating to 600°C (Fig. 4(a)), composition III shows the same three microstructural features as composition V, but the relative amounts differ considerably. The scale consists of a larger fraction of borosilicate glass (c, dark phase) and the mixed MoO_3/SiO_2 matrix (b), and less of the high molybdenum content oxide (a). Up to 750°C (Fig. 4(b)–(d)) oxidation proceeds in much the same manner as for composition V. After volatilization of MoO_3 at 775°C (Fig. 4(e)) the scale on composition III appears different than that of composition V. The matrix structure first observed on composition III at 633°C has formed a smoother scale than seen on composition V. The scale exhibits bimodal porosity, with a few pores ≈ 5 μm in diameter surrounded by porosity on the order of 0.1 μm in size. These pores do not appear to extend completely through the scale to the silicide surface. The appearance of these regions may be due to the thinner scale that forms on $MoSi_2$ grains in the microstructure, resulting in a region of thinner oxide that appears as a pore or depression in the scale surface. XRD patterns of the scale of composition III, as shown in Fig. 5, differ from those for composition V above 800°C. No MoO_3 is detected by XRD above 900°C, in contrast to composition V. In addition, a metallic molybdenum interlayer does not form for oxidation temperatures up to 1000°C for short exposure times. This indicates that silicon and molybdenum are being removed from the interface at the same rate. After 20 min at 1000°C (Fig. 4(g)), the scale shows little sign of additional viscous flow compared to Fig. 4(f). After 40 min at 1000°C, signs of viscous flow become obvious, coincident with the growth of the Mo (100) peak in the XRD spectrum, and formation of a protective scale layer.

Since molybdenum enrichment was detected during XRD analysis of the surface scales, cross-sections of the 100 h oxidized coupons were examined by SEM/EDS (see below). However, neither BSE image contrast nor by X-ray dot mapping revealed the presence of a molybdenum-rich layer on any of the compositions. The molybdenum layer is apparently too thin to be detected by SEM examination.

3.3. Thermo-gravimetric analysis

Fig. 6 shows plots of the mass change on isothermal oxidation at 1000°C in HP air. All specimens exhibited an initial mass gain as the oxidation temperature was

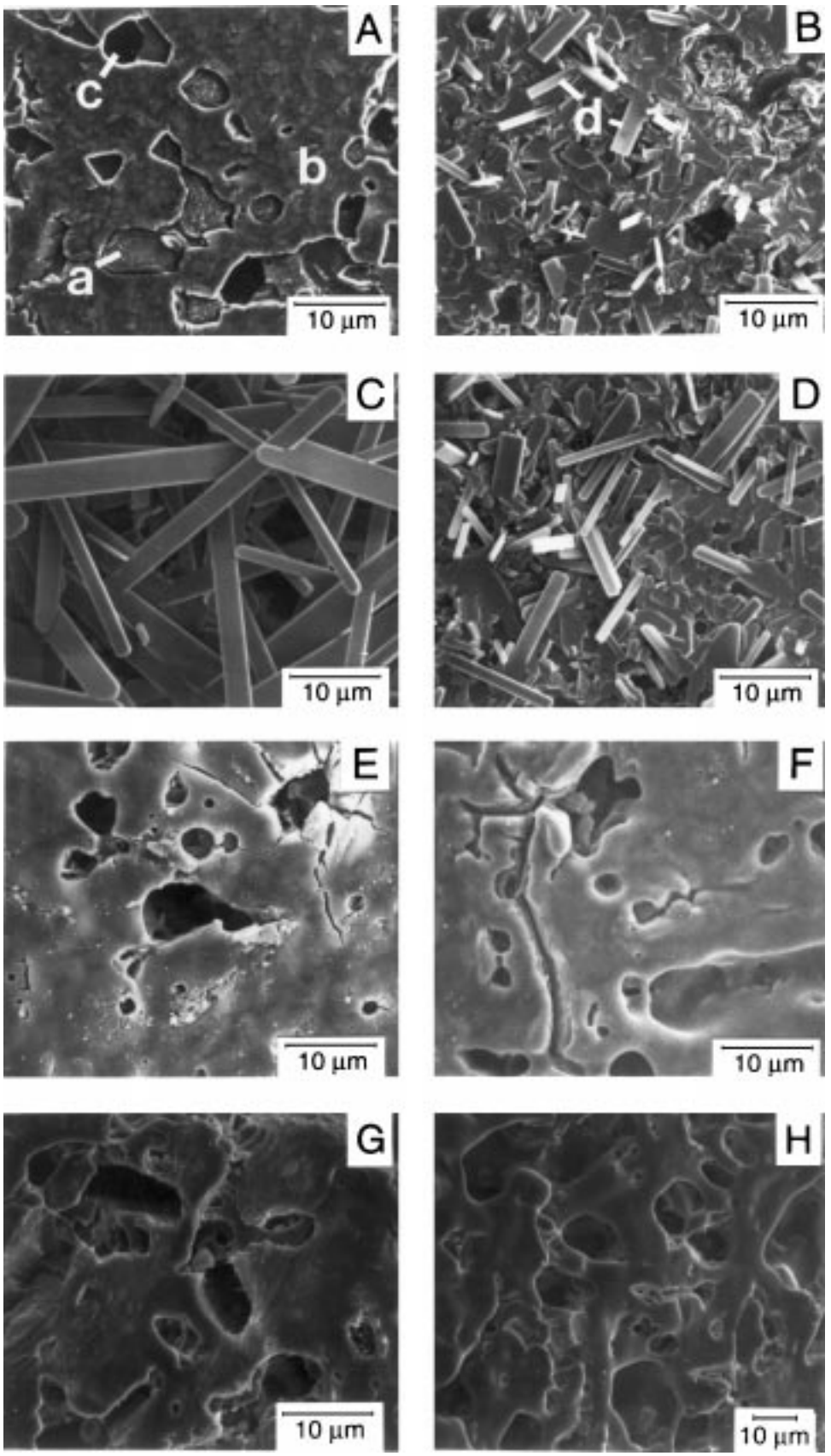

Fig. 4. Formation of the oxide scale on composition III at 600–1000°C. (A) 600°C, (B) 667°C, (C) 725°C, (D) 750°C, (E) 775°C, (F) 1000°C, (G) 1000°C for 20 min, (H) 1000°C for 40 min. Labeling key: a = MoO_3, b = $MoO_3 + SiO_2$, c = borosilicate glass, d = MoO_3 crystals.

ramped past 600°C. There is a rapid mass loss starting at 750°C (Fig. 7), given in Table 2. As seen in Figs. 2–5, the initial mass gain is due to formation of silicon and molybdenum oxides; the mass loss is due to volatilization of molybdenum oxide. Initial mass loss before steady state ranged from 2.8 mg cm^{-2} for composition I to 11.2 mg cm^{-2} for composition V.

After some period of rapid mass loss, oxidation proceeded at a much slower rate. The isothermal portion of the oxidation curves for compositions I–V are shown in Fig. 8. The curves have been shifted to more clearly show the differences in isothermal rates. Oxidation rates, shown in Table 2, were determined by assuming a linear model for oxidation kinetics from 20–100 h. No significance should be given to the choice of a linear model other than to give a comparative mass change rate. Compositions I–III exhibit mass loss over the duration of the oxidation tests. Composition IV shows mass loss over the first 32 h of oxidation followed by a period of almost zero net mass change. Composition V shows a small positive mass change on oxidation.

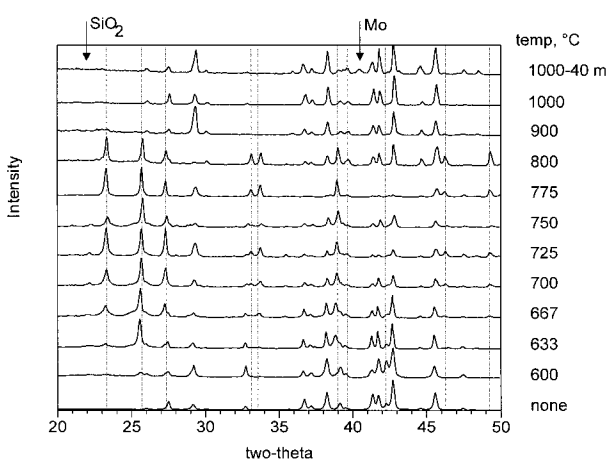

Fig. 5. X-ray diffraction patterns of scale on composition III after oxidation at 600–1000°C. Dashed lines indicate MoO_3. Also indicated are positions of 100% intensity peaks for molybdenum and cristobalite.

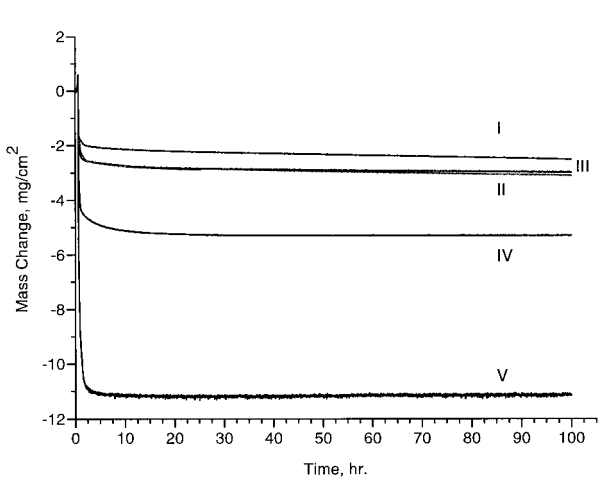

Fig. 6. Mass change on oxidation of specimens I–V at 1000°C.

4. Discussion

Oxidation of all compositions proceeded in two stages, an initial transient period followed by a region of

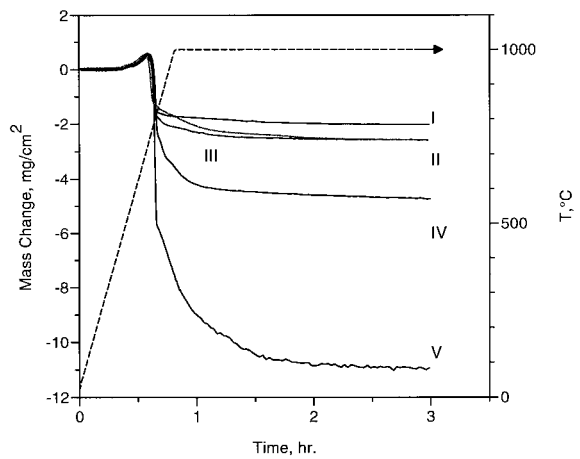

Fig. 7. Initial oxidation of compositions I–V showing mass loss in the initial transient oxidation regime.

Table 2
Boron/silicon ratios, initial mass loss and steady state oxidation rates

Specimen	Atomic B/Si ratio (ICP–AES)	Initial mass loss, mg cm^{-2}	Steady state[a] rate, mg cm^{-2} h^{-1}
I	0.09	2.8	-3.3×10^{-3}
II	0.02	2.2	-3.6×10^{-3}
III	0.14	2.8	-1.9×10^{-3}
IV[b]	0.23	5.3	-5.0×10^{-5}
V	0.24	11.2	$+7.3\times10^{-4}$

[a] 20–100 h.
[b] 30–100 h.

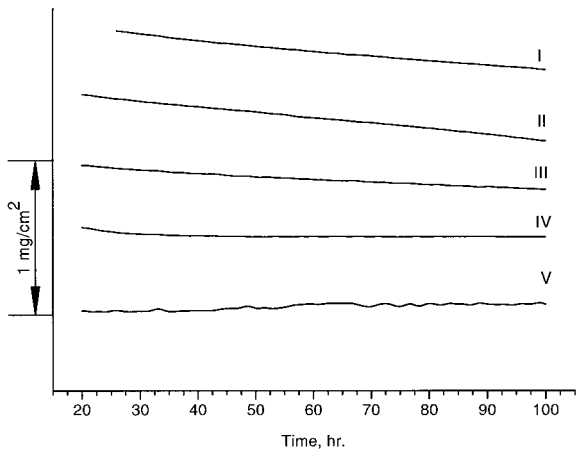

Fig. 8. Isothermal portion of oxidation curves for compositions I–V. Curves have been shifted for ease in comparing relative slopes. $T = 1000$°C.

steady state oxidation. In some cases (I and II) transient mass loss is relatively small and essentially complete by 850°C, indicating rapid formation of a protective scale. In other cases (IV and V) transient mass loss continues well into the isothermal temperature regime.

As the scale initially forms, it contains molybdenum oxide (Figs. 2(a) and 4(a)), which volatilizes to leave a porous scale. The volume fraction of molybdenum oxide initially present in the scale at *ca.* 600°C determines the fractional porosity of the scale after the oxide volatilizes but before viscous flow occurs. Compositions with more Mo_3Si in the microstructure have a larger degree of molybdenum oxide segregation in the scale at 600°C. The scale that forms on Mo_3Si is rich in molybdenum oxide, so that these scales form with a larger pore fraction and larger size pores at 800°C than specimens with little or no Mo_3Si in the microstructure.

Regardless of the magnitude of the initial mass loss, there is a transition to a slower, steady state oxidation regime. The cause of this transition must be the eventual formation of a protective surface layer. The scale that forms may be a continuous protective layer; sealing the substrate surface and allowing only atomic scale diffusion as a means of oxygen transport to the reaction interface. Alternatively a partially protective microporous scale may form, forcing oxygen and oxidation products to flow through a torturous path (by Knudsen diffusion or a similar process) to the substrate surface, slowing transport and thereby reducing the oxidation rate.

If oxidation is limited by oxygen diffusion and the silicon activity at the oxidation interface is sufficient, oxygen partial pressure will be fixed by the Si/SiO_2 equilibrium. Silicon dioxide has a much lower free energy of formation than any molybdenum oxide, the dominant oxidation reaction will be:

$$Mo_5Si_3 + 3O_2 \rightarrow 5Mo + 3SiO_2 \quad (1)$$

A silicon depleted and molybdenum rich interlayer will thus form. It has been shown that SiO_2 can exist in equilibrium with Mo and Mo_5Si_3 so that formation of an Mo_3Si layer is not thermodynamically necessary. [7] Eq. (1) predicts a net mass gain on oxidation. Composition V exhibited an isothermal mass gain and formation of a molybdenum interlayer after ramping to 1000°C, providing evidence that oxidation of composition V at 1000°C is controlled by oxygen diffusion through a completely passivating scale.

On the other hand, if oxidation is not oxygen diffusion limited and the partial pressure of oxygen at the interface is high enough to oxidize molybdenum, oxidation will proceed according to:

$$2Mo_5Si_3 + 21O_2 \rightarrow 10MoO_3(\text{volatile}) + 6SiO_2 \quad (2)$$

Reaction (2) predicts a mass loss due to volatilization of molybdenum oxide (above ≈750°C), and that a metallic molybdenum interlayer will not form. Compositions I and II exhibited a slow steady state mass loss without formation of a molybdenum interlayer (as shown by XRD), so that it is believed that reaction (2) is the dominant oxidation reaction for compositions I and II at 1000°C. Composition IV was an intermediate case, with a transition from mass loss to zero mass change occurring after 30 h of oxidation. In this case, Eq. (1) and Eq. (2) must be competing to yield an essentially zero net mass change.

Important variables to consider when describing the transition to steady state oxidation are scale porosity and scale viscosity. Initial scale porosity and pore size will affect the steady state oxidation rate if viscous flow does not occur to close pores on a reasonable time scale. If viscous flow of the scale to form a coherent passivating layer does occur, then the steady state oxidation rate will be controlled by the diffusion rate of oxygen through the passivating layer. Viscosity (η) of the scale

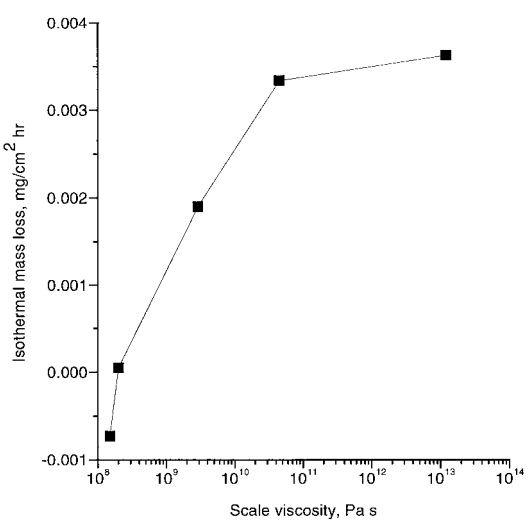

Fig. 9. Isothermal oxidation rate as a function of calculated scale viscosity for compositions I–V. $T = 1000°C$.

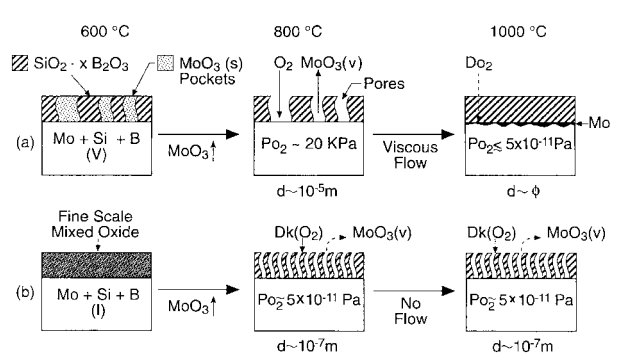

Fig. 10. Schematic of oxidation process. (a) case for formation of porous (low density), low viscosity scale, (b) case for formation of lower porosity, high viscosity scale.

was estimated from the B/Si ratio in the bulk compositions using an empirical equation given by Yan, [8] modified slightly to give a better fit to viscosity data in the composition and temperature range of interest. Fig. 9 shows the variation of isothermal oxidation rate with the estimated viscosity of the scale (at 1000°C). The estimated scale viscosity was calculated assuming that the B/Si ratio in the scale is identical to the initial B/Si ratio of the substrate. The isothermal mass loss rate can be seen to decrease with decreasing estimated scale viscosity.

A schematic representation for the transient oxidation behavior of Mo–Si–B intermetallics was constructed based on the above kinetic and microstructural observations. Fig. 10 shows a diagram which illustrates two extreme cases. Fig. 10(a) shows the case where a low viscosity scale forms initially with large pores and a

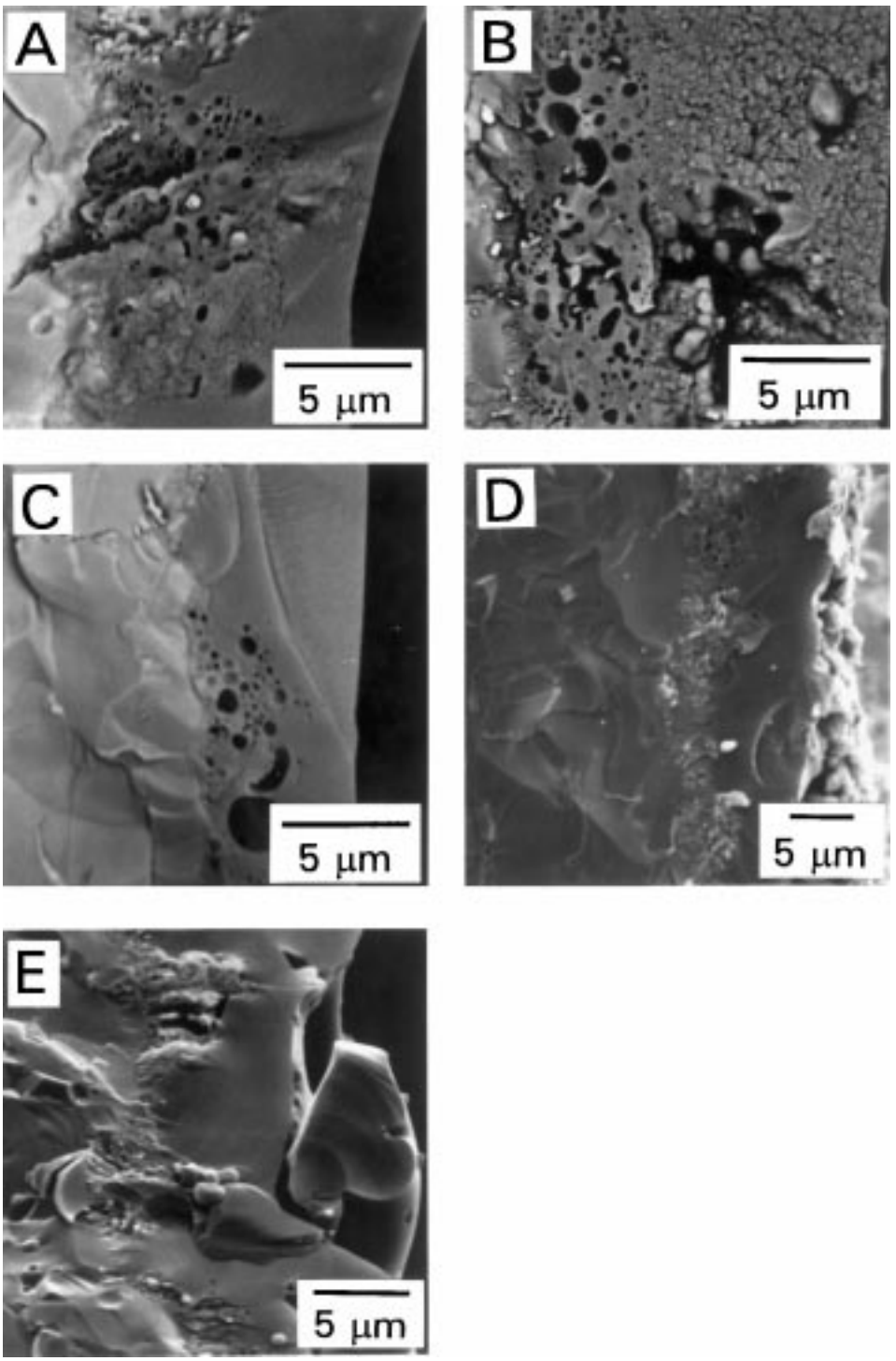

Fig. 11. SEM micrographs of cross section of compositions I–V oxidized at 1000°C for 100 h. (A) I, (B) II, (C) III, (D) IV, (E) V.

large pore fraction. Initially, the scale forms at 600°C with large pockets of almost pure MoO_3, as shown in Fig. 2(a). At 800°C, MoO_3 has volatilized, leaving a network of borosilicate glass with voids on the order of 10 μm in diameter. These voids allow for fast oxygen transport to the interface, causing rapid oxidation and loss of molybdenum via reaction (2). Oxidation of molybdenum continues until densification of the scale by viscous flow closes the pores and forms a coherent oxide layer. After scale porosity is closed the only path for oxygen transport to the interface is by diffusion through borosilicate glass and oxidation kinetics become diffusion controlled. Fig. 10(b) shows the case for a composition that initially forms a low porosity, high viscosity scale. Initially the scale forms as a uniform microstructure of finely divided MoO_3 and borosilicate glass. At 800°C, MoO_3 has volatilized, leaving behind a porous borosilicate glass. The pore size is on the order of 0.1 μm, so that oxygen transport to the interface (by Knudsen diffusion or a similar process) occurs at a much slower rate. Viscous flow does not occur on the time scale of 10^2 h (the duration of the present experiments), so that oxygen diffusion kinetics remain relatively constant. The oxidation rate remains at some value determined by the reactant and/or product transport rate through the porous scale.

Cross-sections of compositions I–V after the 100 h isothermal oxidation tests at 1000°C were analyzed by SEM. As shown in Fig. 11, these micrographs reveal that compositions I–III exhibit porosity within the scale. Composition II shows areas of extensive porosity throughout the scale while compositions I and III showed porosity concentrated at the scale/alloy interface and extending near the scale surface. In contrast, both compositions IV and V exhibit nearly pore-free scales, and these microstructural observations are consistent with a mass loss for compositions I–III and zero loss to mass gain for compositions IV and V. Micrographs taken from the surface of the scales were examined, but external scale roughness precludes determining if the scale forms a continuous, pore-free protective layer across the substrate.

We have previously [2] studied the oxidation kinetics as a function of temperature for a composition similar to III, and found that oxidation changes from mass loss to mass gain behavior between 1050° and 1100°C. Above 1100°C for times of 20–300 h, oxidation kinetics are controlled by diffusion of oxygen through the scale. Given sufficient time and/or temperature, all compositions tested in this study are expected to develop a fully dense scale and oxidation kinetics should be controlled by the rate of oxygen diffusion through the scale. The rate of oxygen diffusion through borosilicate glass increases with boron content [9] so it is expected that isothermal oxidation rates in the diffusion controlled regime will increase with the boron content in the intermetallic.

5. Summary

The oxidation behavior of molybdenum rich Mo–Si–B compositions was studied using X-ray diffraction, thermo-gravimetric analysis, and microscopic observation of the surface at different stages of scale growth. Microstructure of the scale and hence the oxidation behavior of the intermetallics were related to chemical composition. A schematic representation for the transient oxidation behavior was devised based on the initial pore formation and subsequent reflow behavior of the scale. The transient oxidation rate is likely controlled by the transport of oxygen through a porous scale layer.

Acknowledgements

Ames Laboratory is operated for the US Department of Energy by Iowa State University under contract number W-7405-ENG-82. This research was supported by the Office of Basic Energy Science, Materials Science Division.

References

[1] Anton DL, Shah DM. High temperature properties of refractory intermetallics. Mat Res Soc Symp Proc 1991;213:733–9.
[2] Meyer MK, Akinc M. Oxidation behavior of boron modified Mo_5Si_3 at 800–1300°C. J Am Ceram Soc 1996;79(4):938–44.
[3] Zhang SL, Ghez R, d'Heurle FM. A mathematical model for silicide oxidation. J Electrochem Soc 1990;137(2).
[4] D'Heurle FM, Crs A, Framptom RD, Irene EA. Thermal oxidation of silicides on silicon. Phil Mag 1987;B55(2):291–308.
[5] Bartlett RW, McCamont JW, Gage PR. Structure and chemistry of oxide films thermally grown on molybdenum silicides. J Am Ceram Soc 1965;48(11):551–8.
[6] Berkowitz-Mattuck JB, Dils RR. High-temperature oxidation: II. Molybdenum silicides. J Electrochem Soc 1965;112(6):583–9.
[7] Beyers R. Thermodynamic considerations in refractory metal–silicon–oxygen systerns. J Appl Phys 1984;56(1):147–52.
[8] Yan MF, MacChesney JB, Nagel SR, Rhodes WW. Sintering of optical wave-guide glasses. J Mater Sci 1980;15:1371–8.
[9] Schlichting J. Oxygen transport through glass layers formed by a gel process. J Non-Crystall Solids 1984;63:173–81.